Chemical Engineering Science 309 (2025) 121467

Contents lists available at ScienceDirect

Chemical Engineering Science

journal homepage: www.elsevier.com/locate/ces

Benchmark case for the inverse determination of adsorption parameters using lattice Boltzmann methods and gradient-based optimization

Shota Ito [a,b,*], Simon Großmann [a,c], Fedor Bukreev [a,b], Julius Jeßberger [a,c], Mathias J. Krause [a,b,c]

[a] Lattice Boltzmann Research Group, Karlsruhe Institute of Technology, Karlsruhe, Germany
[b] Institute of Mechanical Process Engineering and Mechanics, Karlsruhe Institute of Technology, Karlsruhe, Germany
[c] Institute for Applied and Numerical Mathematics, Karlsruhe Institute of Technology, Karlsruhe, Germany

ARTICLE INFO

Keywords:
Inverse problems
Lattice Boltzmann method
Computational fluid dynamics
Gradient-based optimization

ABSTRACT

This work proposes a parameter identification framework for determining adsorption model parameters from given concentration curves. Therein, an inverse problem involving a coupled system of partial differential equations is solved numerically by combining lattice Boltzmann methods and gradient-based optimization. The framework is validated for a constructed benchmark case where the concentration data for a batch reactor is obtained via the analytical solution or through simulations. Utilizing the benchmark case, we demonstrate the grid independence of the optimization problem when using simulation data and second order convergence of the identified parameters when the analytical solution is used as the input. From simulation data, the framework recovered the isotherm constant with an initial relative error from 67 % to machine precision accuracy in 13 optimization steps. When artificial noise signals are imposed onto the input data with an intensity of SNR = 2, the final relative error regarding the parameters yields 2 %.

1. Introduction

Adsorption processes are present in various applications, for instance in wastewater treatment (Berg et al., 2005). Here activated carbon is used to remove dissolved organic matter and organic micro-pollutants and phosphate is removed by either aluminium oxide or iron hydroxide (Worch, 2021). The amount of adsorbed substances thereby depends on various parameters such as the concentration of the different substances, temperature, the adsorbent, its properties, and on the general transport phenomena, such as the convective flow velocity. A crucial state of the process is the equilibrium state at which the maximal possible amount is adsorbed. The parameterized relation describing the respective equilibrium relation, considered at constant temperature, is referred to as the adsorption isotherm and is therefore essential for understanding the adsorption process. However, obtaining information on the equilibrium state can be challenging as several experiments with expert knowledge might be required and have to be predicted (Worch, 2021). There exists several models approximating the adsorption isotherm by a parameterized expression ranging from linear models regarding the solute concentration, such as the Henry-isotherm, to more complex non-linear models such as the Langmuir or Freundlich isotherm (Glueckauf and Coates, 1947). An overview for further adsorption models is given in Worch (2021) for interested readers.

Due to advancements in computational methods, numerical approaches are utilized to address adsorption processes as an alternative to experimental studies (Bukreev et al., 2023; Worch, 2012; Bonvin, 1998; Grigoriev et al., 2020). The lattice Boltzmann method (LBM) originating from the kinetic theory has been proven to be a popular approach to solve complex coupled systems of macroscopic transport equations (Krause et al., 2021; Bukreev et al., 2023; Ito et al., 2024). Furthermore, the discrete formulation of the solved equation shows high suitability towards massive parallelization on high performance computing systems making LBM an efficient method for numerical studies (Simonis, 2023; Krause et al., 2021). However, the set up of a successful simulation still requires model parameters to conduct the study in the first place, such that the interest for an alternative approach to determine the model parameters remains.

A promising approach to identify adsorption model parameters is to formulate an inverse problem and solving it using optimization, as it has been successfully employed in previous works (Ito et al., 2024; Klemens et al., 2018, 2020a,b; Krause et al., 2013). Therein, the model parameter are determined inversely from reference concentration data by

* Corresponding author.
E-mail address: shota.ito@kit.edu (S. Ito).

https://doi.org/10.1016/j.ces.2025.121467
Received 4 October 2024; Received in revised form 25 February 2025; Accepted 28 February 2025
Available online 2 March 2025

minimizing the deviation of the reference and simulated results where the reference data could be obtained experimentally. The success of the optimization problem is measured by the objective function which evaluates the distance between reference and simulation concentration data. Joshi et al. (2013) addressed parameter identification problems in virus transport, based on adsorption mechanisms. Therein, a finite volume scheme is employed combined with the Levenberg-Marquardt algorithm. In Ito et al. (2024), reaction kinetics parameters are successfully identified reversely from concentration distributions for a reactive flow problem showing the promising possibilities of this approach. Recently, Grigoriev et al. (2020) investigate the parameter identification approach for adsorption and desorption parameters for the Langmuir isotherm in the pore-scale by combining finite element methods and stochastic methods. However, the application of inverse problems for complex physical systems as it is often the case in adsorption processes remains still rarity in the literature. One reason for this could be the challenge of solving efficiently the non-liner system of coupled partial differential equations as optimization constraints. Further challenge presents the ill-posed problem formulation resulting in ambiguous solutions of the inverse problem especially in the presence of noise signals in the input data.

To address this issue, we propose a combined framwork of LBM and gradient-based optimization where the objective sensitivities are obtained by forward mode of automatic differentiation. Iterative parameter adjustment is performed by the framework performing LBM simulations for each function and gradient evaluation. Compared to Grigoriev et al. (2020), a quasi-Newton algorithm is used to automatize the process of converging effectively towards the desired model parameters. The choice of LBM combined with a gradient-based approach is mainly motivated by the computational efficiency of the LBM algorithm and the relatively less performed function evaluations compared to heuristic optimization approaches. Here, LBFGS (Liu and Nocedal, 1989; Byrd et al., 1995) is employed as the optimization algorithm where the whole framework is realized by in the open source library OpenLB (Krause et al., 2021; Kummerländer et al., 2024). For the adsorption model, the linear Henry-isotherm model is applied for the batch reactor set up introduced by Bukreev et al. (2023) where the current manuscript documents its follow-up work. We constructed a benchmark validation case for the model parameter identification problem in adsorption processes for the batch reactor case to validate our framework. Any isotherm model can be replaced for the Henry-isotherm model as well as any adsorption or transport model can be applied such that there is no loss of generality in the presented benchmark case. Furthermore, the presented method is analyzed regarding accuracy of the recovered parameters, influence of the grid resolution, robustness of the inverse problem by testing various initial guesses, and the presence of noise signals. The current work differs from the work of Grigoriev et al. (2020) in terms of the chosen adsorption model as ours is acting on the macroscopic scale and in the formulation of the objective functional by encouraging spatially distributed input data for the inverse problem to counteract the ill-posedness of the problem (Ito et al., 2024).

The presented manuscript is structured as below. In Section 2 the inverse determination of adsorption model parameters is formulated as an optimization problem. The LBM used to obtain the concentration curve by approximating the coupled system of conservation equations as optimization constraints as well as the optimization algorithms are explained. Section 3 introduces the employed quality measures used for analysis of the followed numerical experiments wherein the framework is investigated regarding the above mentioned aspects by conducting the corresponding numerical tests. Finally, a short summary and conclusion is given in Section 4.

2. Methodology

This chapter is dedicated to formulate the inverse problem which we aim to solve as well as the methods we use to solve the problem numerically. In Section 2.1 the inverse problem is formulated as an optimization problem introducing the applied objective and constraint functions. Next, Section 2.2 describes the LBM to approximate the constraint function together with the modelling of the adsorption processes. Finally, Section 2.3 introduces the implemented gradient-based optimization framework with the entire workflow for the parameter identification of adsorption model parameters.

2.1. Problem formulation

The inverse problem in this work can be formulated as an optimization problem where parameters of the adsorption isotherm function are obtained from reference solute concentration curves $c_s^* : \Omega \times I \to \mathbb{R}$. In the most simple adsorption model, the solute concentration curve depends solely on the Henry-isotherm K_H (Hashimoto and Miura, 1976; Worch, 2008, 2021), i.e., $c_s : \Omega_{\triangle x} \times I_{\triangle t} \to \mathbb{R}$ with $c_s = f(K_H)$. The flow domain and the corresponding discretized domain is denoted by Ω and $\Omega_{\triangle x}$, as well as the time domains by I and $I_{\triangle t}$, respectively. Note, that the spatial positions of the measurement data $\mathbf{x}^* \in \Omega$ do not necessarily correlate to the grid positions $\mathbf{x} \in \Omega_{\triangle x}$ in the simulation such that interpolation can be required to evaluate the deviation. The objective function of the current optimization problem can be written as

$$\min_{\boldsymbol{\alpha}} J(c_s, \boldsymbol{\alpha}) = \int_I \int_{\Omega^*} (c_s^* - c_s(\boldsymbol{\alpha}))^2 \mathrm{d}\mathbf{x}^* \mathrm{d}t, \tag{1}$$

where $\boldsymbol{\alpha}$ is the control vector holding the adsorption model parameters which are to be determined, e.g., the Henry-isotherm K_H. In order to get the solute concentration from the set adsorption parameters, the adsorption model of Bukreev et al. (2023) is used. That is, a coupled system of partial differential equations (PDE) is solved, given as

$$\mathbf{G}(f, \boldsymbol{\alpha}) = \begin{cases} \boldsymbol{\nabla}_{\mathbf{x}} \mathbf{u}, \\ \rho \partial_t \mathbf{u} + \rho \mathbf{u} \cdot \boldsymbol{\nabla}_{\mathbf{x}} \mathbf{u} - \nu \boldsymbol{\Delta}_{\mathbf{x}} \mathbf{u} + \frac{1}{\rho} \boldsymbol{\nabla}_{\mathbf{x}} p, \\ \partial_t c_s + \mathbf{u} \boldsymbol{\nabla}_{\mathbf{x}} \cdot c_s - D_s \boldsymbol{\Delta}_{\mathbf{x}} c_s - S_{\text{ads}}(\boldsymbol{\alpha}), \\ \partial_t c_p + \mathbf{u} \boldsymbol{\nabla}_{\mathbf{x}} \cdot c_p - D_p \boldsymbol{\Delta}_{\mathbf{x}} c_p, \\ \partial_t c_q + \mathbf{u} \boldsymbol{\nabla}_{\mathbf{x}} \cdot c_q - D_q \boldsymbol{\Delta}_{\mathbf{x}} c_q - S_{\text{ads}}(\boldsymbol{\alpha}), \end{cases} \tag{2}$$

where the first two lines are the Navier-Stokes equation (NSE) for the fluid flow and the following three lines advection-diffusion equations (ADE) for modelling the passive scalar transport of solute, adsorbent particles, and particle loading, translated into a concentration via $c_q = c_p q$ (Bukreev et al., 2023). For choosing a sufficiently small diffusion constant D_q, the loading q is transported equally as the particle concentration c_p due to the identical advection velocity obtained from the NSE. Introducing a diffusion term in the transport of particle loading, enables the inclusion of different contributions such as diffusion or mixing and allow the efficient discretization of the ADE via a LBM. The sink term S_{ads} in the transport equation of the solute incorporate the mass transfer due to adsorption from the dispersed state and adds its contribution to the transport equation of the particle loading concentration as shown in (2). That is, the adsorbent particles are resolved on sub-grid scale and the entities such as particle loading are volume-averaged over a numerical grid cell. Analogously to the prior work, we assume that all modeled particles are identical, have the same structure and simulate homogeneous adsorption in the dispersed phase. Furthermore, homogeneous diffusion is assumed by scalar diffusion coefficients. The reader is advised to refer to Bukreev et al. (2023) for a more detailed description of the coupled system of the governing equations.

For the adsorption, the linear driving force (LDF) model (Glueckauf and Coates, 1947) described by the previous work (Bukreev et al., 2023) is used where the following set of equations are solved

$$c_p \partial_t q = -\partial_t c_s, \tag{3}$$

$$\partial_t q = k_s^* \left(q^{\text{eq}} - q\right), \tag{4}$$

$$q^{\text{eq}} = K_H c_s^{\text{eq}}, \tag{5}$$

$$q(t=0) = 0, \quad c_s(t=0) = c_{s,0}, \tag{6}$$

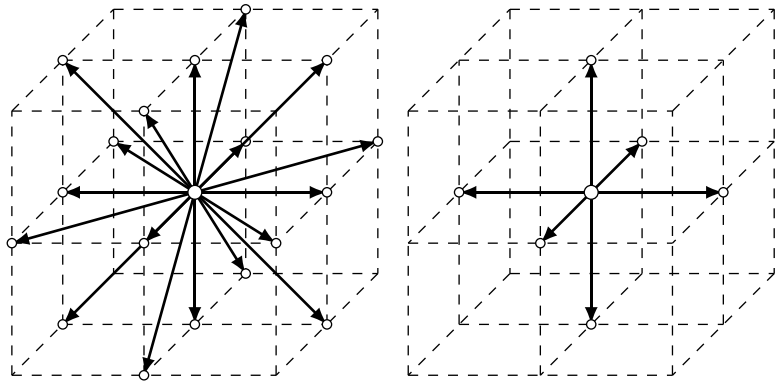

Fig. 1. Schematic view of the $D3Q19$ (left) and $D3Q7$ (right) discrete velocity set. The discrete velocities are depicted as arrows.

where k_s^* is the surface mass transfer coefficient, q^{eq} the surface equilibrium loading, and $c_{s,0}$ the initial solute concentration. The surface mass transfer coefficient k_s^* is related to the adsorbent particle radius r_p over $k_s^* = 15 D_s^{\mathrm{eq}} / {r_p}^2$ where D_s^{eq} is the surface diffusion constant. The Eq. (3) gives the solute mass balance at the adsorbent surface, (4) the particle internal mass transport of the adsorbed solute, (5) the linear Henry isotherm model, and (6) the initial conditions. If film diffusion should be considered, the LDF model can be extended by replacing (5) by

$$c_p k_s (q^{\mathrm{eq}} - q) = k_f (c_s - c_s^{\mathrm{eq}}), \tag{7}$$

where k_s and k_f are surface and film transport coefficient, respectively. For simplicity, in this work film diffusion is neglected and (5) is used. Inserting all equations above into the mass balance (3) and by setting $S_{\mathrm{ads}} = -\mathrm{d}c_s/\mathrm{d}t$ yields

$$S_{\mathrm{ads}} = \frac{15 D_s^{\mathrm{eq}}}{{r_p}^2} c_p \left(K_H c_s^{\mathrm{eq}} - q \right). \tag{8}$$

Note, the appearance of the isotherm coefficient in (8) which is the control variable in the optimization problem. For more detailed information about the adsorption model, the authors refer to our previous work (Bukreev et al., 2023) as well as further works as (Hashimoto and Miura, 1976; Worch, 2008, 2021).

Finally, by minimizing (1) while fulfilling $\mathbf{G} = 0$ by solving the system of PDEs in (2), the isotherm coefficient can be determined inversely from reference solute concentration curves. In future works, the reference curves are obtained from experimental measurements. However, as a proof of concept of our numerical framework, in this preliminary work the reference curve is given by an analytical solution in the batch reactor case or simulated data is used.

2.2. Lattice Boltzmann method

The constraint functions in (2) are solved using a LBM with the multi-distribution function approach (Guo et al., 2002). That is, all equations are sharing the same grid positions $\mathbf{x} \in \Omega_{\triangle x}$ on a homogeneous lattice with the stencil width of $\triangle x$. For the NSE the lattice BGK-Boltzmann equation is solved on each grid position, given as (Krause et al., 2021)

$$f_i(\mathbf{x} + \boldsymbol{\xi}_i \triangle t, t + \triangle t) = f_i(\mathbf{x}, t) - \frac{\triangle t}{\tau} (f_i(\mathbf{x}, t) - f_i^{\mathrm{eq}}(\mathbf{x}, t)), \tag{9}$$

where f_i is the particle distribution function, $\boldsymbol{\xi}_i$ the discrete particle velocity, τ the relaxation time, and f_i^{eq} the equilibrium distribution function. For the ADEs, analogously lattice BGK-Boltzmann equations are solved with an additional source term, given as (Bhatnagar et al., 1954)

$$g_i(\mathbf{x} + \boldsymbol{\xi}_i \triangle t, t + \triangle t) = g_i(\mathbf{x}, t) - \frac{\triangle t}{\tau_g} (g_i(\mathbf{x}, t) - g_i^{\mathrm{eq}}(\mathbf{x}, t)) + \triangle t S_i. \tag{10}$$

where g_i is the particle distribution function, τ_g the relaxation time, and g_i^{eq} the equilibrium distribution function for the ADE. The subscript i refers to the discrete velocity directions according to the applied discretization model, where for the NSE the $D3Q19$ model and for the ADEs the $D3Q7$ model is used (Yoshida and Nagaoka, 2010), both depicted in the schematic in Fig. 1. Using the zeroth order moment (ADE) and zeroth and first order moments (NSE), the NSE and ADE are formally recovered with second order consistency in the incompressible limit of a Chapman-Enskog expansion. Further, an estimation of the consistency order, e.g. by Taylor expansions of LBMs for the NSE and the ADE is provided in Simonis and Krause (2022) and Simonis (2023), Simonis et al. (2023), respectively. Completing the convergence of the individual models, complementary stability analyses for LBMs approximating the NSE and ADE are provided in Simonis (2023), Simonis et al. (2020, 2021), Dapelo et al. (2021). Convergence up to second order of LBM specifically for RADEs has been numerically observed in Ito et al. (2024). Here, the NSE and ADE are coupled via the velocity and form the targeted PDE system. The contributions of the source term in the discrete velocity directions equals to $S_i = (1 - 1/2\tau_g) w_i S_{\mathrm{ads}}$ (Yoshida and Nagaoka, 2010; Seta, 2013; Gruszczyński et al., 2023), where w_i are the weighting terms of the applied velocity discretization model, given in Table 1. The equilibrium distribution in the collision operator in (9) is given as

Table 1
Lattice discretization parameters.

Directions i	Discrete particle velocity $\boldsymbol{\xi}_i$	Weights w_i
0	$(0, 0)$	1/3
$1, 2, \ldots, 6$	$(\pm 1, 0, 0), (0, \pm 1, 0), (0, 0, \pm 1)$	1/18
$7, 8, \ldots, 18$	$(\pm 1, \pm 1, 0), (\pm 1, 0, \pm 1), (0, \pm 1, \pm 1)$	1/36
0	$(0, 0)$	1/4
$1, 2, \ldots, 6$	$(\pm 1, 0, 0), (0, \pm 1, 0), (0, 0, \pm 1)$	1/8

$$f_i^{\mathrm{eq}}(\mathbf{x}, t) = w_i \rho \left(1 + \frac{\boldsymbol{\xi}_i \cdot \mathbf{u}}{{c_s}^2} + \frac{(\mathbf{u} \cdot \boldsymbol{\xi}_i)^2}{2{c_s}^4} - \frac{\mathbf{u} \cdot \mathbf{u}}{2{c_s}^2} \right), \tag{11}$$

and in (10) as

$$g_i^{\mathrm{eq}}(\mathbf{x}, t) = w_i c \left(1 + \frac{\boldsymbol{\xi}_i \cdot \mathbf{u}}{{c_s}^2} \right), \tag{12}$$

where the lattice speed of sound is $c_s = 1/\sqrt{3}$ as the stencil width and discrete time step is set to unity. The macroscopic entities of the NSE can be accessed via the statistic moments, given as

$$\rho = \sum_{i=0}^{19} f_i, \tag{13}$$

$$\mathbf{u} = \frac{1}{\rho} \sum_{i=0}^{19} \boldsymbol{\xi}_i f_i, \tag{14}$$

$$\triangle p = {c_s}^2 (\rho - \rho_{\mathrm{ref}}). \tag{15}$$

Here, ρ_{ref} is a reference density of the fluid or a reference pressure level converted to the density. The transported macroscopic concentrations can be computed over

$$c = \sum_{i=0}^{6} g_i + \frac{\triangle t}{2} S_{\text{ads}}. \tag{16}$$

Note, that computing S_{ads} requires c_p and c_q for q as shown in (8), which are calculated by using the uncorrected moment, i.e., $\tilde{c} = \sum_{i=0}^{6} g_i$. By applying diffusive scaling, convergence orders up to two can be achieved this way as otherwise an implicit equation is required to solve for (16) as stated in Seta (2013), Gruszczyński et al. (2023). Thus, in all conducted numerical experiments, diffusive scaling is applied. The relaxation time is connected to the viscosity in (9) and to the diffusivity coefficient in (10) over

$$\nu = {c_s}^2 \left(\tau - \frac{\triangle t}{2} \right), \tag{17}$$

$$D = {c_s}^2 \left(\tau_g - \frac{\triangle t}{2} \right). \tag{18}$$

The LBM models in (9) and (10) are so called single-relaxation-time (SRT) models, where stability issues have been reported such as in Wang et al. (2015). However, the proposed framework is designed to be replaceable in terms of used LBM model and in the following numerical experiments no stability issues are observed which is why the SRT model has been applied due to its simplicity.

2.3. Optimization framework

The previous section outlined how the coupled system of PDEs for the constraints is solved, only the utilized optimization algorithm is missing. In order to solve the optimization problem in (1) numerically, an iterative gradient-based optimization algorithm is used. Algorithm 1 shows the performed steps by the implemented parameter identification framework. First, the algorithm starts from an initial guess of the adsorption model parameters $\boldsymbol{\alpha}^0$ and compute the solute concentration by the introduced LBM, where m corresponds to the mth optimization step. That is, (9) and (10) are solved yielding the solute concentration curve for the current $\boldsymbol{\alpha}^m$. Using this solution, the objective function can be computed in each iteration step explicitly by

$$J^m({c_s}^m, \boldsymbol{\alpha}^m) = \sum_{t \in I_{\triangle t}} \sum_{\mathbf{x} \in \Omega_{\triangle x}} \left(c_s^*(\mathbf{x}, t) - c_s(\mathbf{x}, t, \boldsymbol{\alpha}^m) \right)^2. \tag{19}$$

In the next step, the gradients of the objective function $\mathrm{d}J^m/\mathrm{d}\boldsymbol{\alpha}$ are computed using the forward mode of automatic differentiation (f-AD). The f-AD was successfully tested and applied in former studies (Ito et al., 2024; Jeßberger et al., 2022; Krause and Heuveline, 2013). The interested reader, regarding AD in general or the internal implementation of AD in OpenLB used in this work, is referred to the concise introduction by Griewank and Walther (2009) or the works of Ito et al. (2024) or Jeßberger et al. (2022), respectively. The algorithm terminates when the value of the objective function or the L_2-norm regarding its total derivative is lower than a user-specified threshold $\epsilon > 0$. After obtaining the gradients, the control parameters are updated by the quasi-Newton method LBFGS (Liu and Nocedal, 1989) which approximates the second derivative and computes $\triangle \boldsymbol{\alpha}^m$ with

$$\triangle \boldsymbol{\alpha}^m = s^m \mathbf{d}^m, \tag{20}$$

where s^m is the step size and $\mathbf{d}^m$ the descent direction of the current optimization step m. Armijo and Wolfe rules are applied to find appropriate step sizes s^m balancing stability and convergence speed (Byrd et al., 1995). Therein, the appropriate step size is found by applying iterative changes, i.e., an additional inner loop performs several function or gradient evaluations performing LBM simulations. When both rules are satisfied, the adsorption model parameters $\boldsymbol{\alpha}$ are updated according to $\boldsymbol{\alpha}^{m+1} = \boldsymbol{\alpha}^m + \triangle \boldsymbol{\alpha}^m$ and the current step is counted as a valid optimization step. After updating the control variables, the algorithm returns to step 3, repeating the steps until satisfying the termination condition.

Algorithm 1 Gradient-based optimization algorithm with f-AD and step control.

1: **procedure** MINIMIZE($J({c_s}, \boldsymbol{\alpha})$)
2: Choose initial guess α^0, maximal number iterations $m_{\max}, k_{\max}$, and convergence tolerance ε
3: **repeat** ▷ For $m = 0, 1, 2, \ldots, m_{\max}$
4: Solve **G** with LBM
5: Compute gradients reg. controls with f-AD
6: Compute $\mathrm{d}J/\mathrm{d}\alpha$ using results from step 4 and 5
7: Compute descent direction via L-BFGS using result from step 6
8: **repeat** ▷ For $k = 0, 1, 2, \ldots, k_{\max}$
9: Choose new step size $s^{m,k}$
10: Check if valid step for $\delta\boldsymbol{\alpha}^{m,k} = s^{m,k}\mathbf{d}^m$
11: **until** Valid step size found **or** $k = k_{\max}$
12: Update controls $\boldsymbol{\alpha}^{m+1} = \boldsymbol{\alpha}^m + \delta\boldsymbol{\alpha}^m$
13: **until** $J({c_s}^m, \boldsymbol{\alpha}^m) < \varepsilon$ **or** $(\mathrm{d}J/\mathrm{d}\boldsymbol{\alpha})({c_s}^m, \boldsymbol{\alpha}^m) < \varepsilon$ **or** $m = m_{\max}$ ▷ Terminating condition
14: **end procedure**

3. Constructing a benchmark case: batch reactor

This chapter introduces a benchmark case which validates and demonstrates the capabilities of the presented framework for inverse determination of adsorption model parameters. The performance of our framework regarding number of parameters, type of input data, grid resolution, and presence of noise signals are investigated.

3.1. Numerical set up

The batch reactor is implemented as a cube with periodic boundaries in all directions with neglected velocity distributions. That is, for the batch reactor, the constraint function in (2) can be reduced to the ADEs. However, to not lose generality, the constraint function in Section 2.1 contains the NSE to allow the application of the proposed framework for further studies, such as fixed bed reactors. In this presented work, we focus on the construction of the benchmark case, i.e., the batch reactor. By assuming spatially uniform conditions, the spatial dimension can be omitted which further reduces the complexity, which suits the purpose of a simple validation case. For this case, an analytical solution for the solute concentration curve has been derived by Worch (2021). Following the LDF model, the transient change of the dimensionless concentration $X = c_s/c_{s,0}$ can be written as

$$X(T) = \frac{1}{D_b + 1} + \frac{D_b}{D_b + 1} e^{(-(D_b+1)T)}, \tag{21}$$

with the distribution factor

$$D_b = \frac{c_p q_0^{\text{eq}}}{c_{s,0}}, \tag{22}$$

with $q_0^{\text{eq}} = K_H c_{s,0}$ and the dimensionless time

$$T = k_s^* t. \tag{23}$$

The batch reactor is realized as a cube $0.1 \times 0.1 \times 0.1$m as the side lengths resolved by 20 numerical cells each. In all simulations the relaxation time of all ADEs are set to 0.695 and a time span of 15s is computed. Details on the effects of the relaxation time and the convergence of the adsorption model are provided in the previous work (Bukreev et al., 2023). The process parameters and material properties that were used in the simulations are listed in Table A.1. The simulation setup parameters are summarized in Table 2 and the simulation domain is illustrated in Fig. 2. For the validation, *a-priori* chosen adsorption model

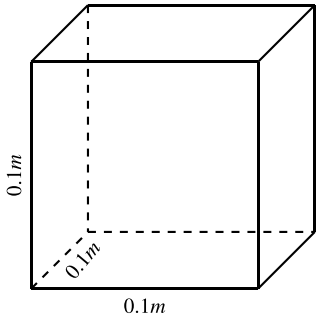

Fig. 2. Simulation domain for the batch reactor.

Table 2
Simulation parameters for the batch reactor (Bukreev et al., 2023).

Parameter		Value	Unit
Simulation time	t	15	s
Characteristic length	L	0.1	m
Resolution of side length	N	20	
Relaxation time	τ_g	0.695	

parameters, hereafter referred to as the reference parameters $\boldsymbol{\alpha}^*$ are used to produce the input concentration curves for the optimization. That is, the optimization framework requires some reference concentration curves c_s^* which are obtained either via the analytical solution given in (21) or by using simulated concentration curves computed with the reference parameters. Both the analytical solution and the reference simulation are computed using the parameters shown in Table A.1. The goal is therefore to recover the originally set reference parameters from those input concentration curves. The minimized objective is equal to the L_2-norm of the absolute error as shown in (1) and can be used as the quality measure for the identified parameters. For the terminating condition, a lower threshold is defined as $\epsilon = 10^{-10}$ for the L_2-norm of the total derivative vector. In the following results, the Henry-isotherm constant and the particle radius is determined from the concentration curves, i.e.,

$$\boldsymbol{\alpha}^* = (K_H, r_p)^{\mathrm{T}}. \tag{24}$$

If not stated differently, the initial guesses regarding the determined parameters are given as

$$\boldsymbol{\alpha}^0 = (15\mathrm{L/g}, 1.0 \cdot 10^{-5}\mathrm{m})^{\mathrm{T}}. \tag{25}$$

The control parameter for the particle radius is constrained to be $r_p > 10^{-7}$m to prevent the optimization framework assigning values leading to instabilities in the simulations.

3.2. Quality measures

In order to analyze the numerical results quantitatively, the following quality measures are utilized in the validation process. The objective function in (19) gives a good indication of how close the computed concentration curve is to the reference curve. To make the objective comparable for different resolutions, the objective value obtained via (19) is normed by the number of grid cells and discrete time steps, i.e., $J^m/N_{I_{\triangle t}}$, where $N_{I_{\triangle t}}$ is the resolution of the time space. To assess the quality of a determined parameter, the relative error to the reference parameter can be computed by

$$\left|\triangle\alpha^m_{\mathrm{rel}}\right| = \left|\frac{\alpha^* - \alpha^m}{\alpha^*}\right|. \tag{26}$$

When multiple parameters are identified, the norm the error vector is used, given as

$$\left|\left|\triangle\boldsymbol{\alpha}^m_{\mathrm{rel}}\right|\right|_{L_2} = \left|\left|\frac{\boldsymbol{\alpha}^* - \boldsymbol{\alpha}^m}{\boldsymbol{\alpha}^*}\right|\right|_{L_2}, \tag{27}$$

where the L_2-norm is used.

3.3. Results

This section shows the obtained results for the batch reactor case. Several aspects has been addressed such as grid influence, number of identified parameters, sensitivity regarding the initial guess, and the introduction of noise signals in the reference data.

3.3.1. Grid influence

We tested two approaches to obtain the input data for the optimization framework. That is, either the analytical solution is used or a reference simulation is performed with the reference parameters $\boldsymbol{\alpha}^*$ to produce the reference concentration curve. For both cases, the influence of the numerical grid resolution is investigated for the resolutions $N = \{10, 20, 40, 80\}$, leading in halving the step size $\triangle x$ in each step. As diffusive scaling is applied, the relaxation time remains constant in all simulations. The grid convergence study for the batch reactor simulation has been done in the previous study (Bukreev et al., 2023) and showed second order convergence in the diffusive scaling. For both cases, the Henry-isotherm constant has been identified with the initial guess as given in (25) and the particle radius has not been changed from the reference value given in Table A.1.

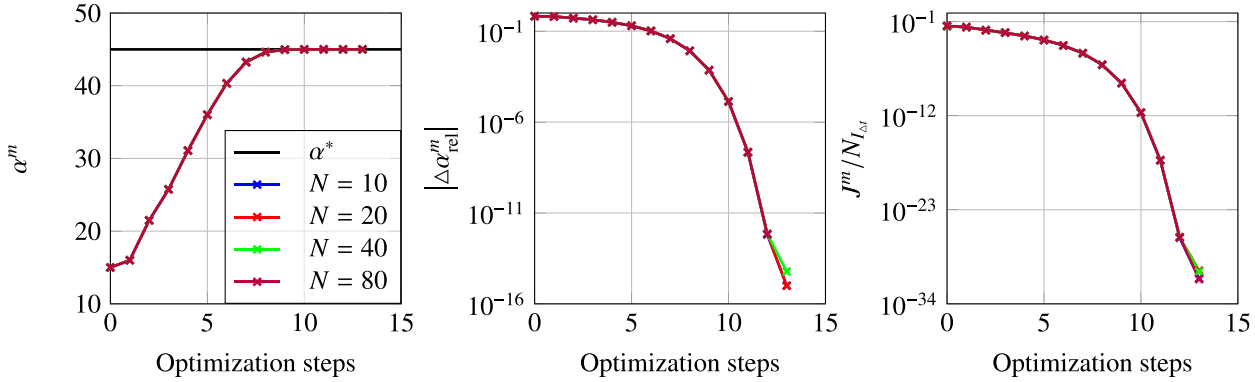

(a) Controls over optimization steps. (b) Rel. error controls over optimization steps. (c) Normed objective over optimization steps.

Fig. 3. Development of the controls and objective function over the performed optimization steps. The reference concentration curve is produced by a reference simulation using the reference controls from Table A.1.

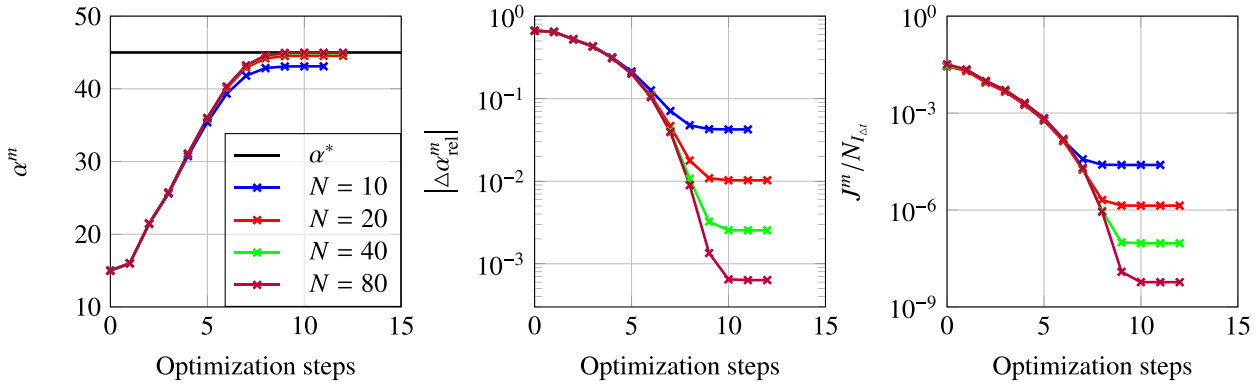

(a) Controls over optimization steps. (b) Rel. error controls over optimization steps. (c) Normed objective over optimization steps.

Fig. 4. Development of the controls and objective function over the performed optimization steps. The reference concentration curve is produced by the analytical solution from (21).

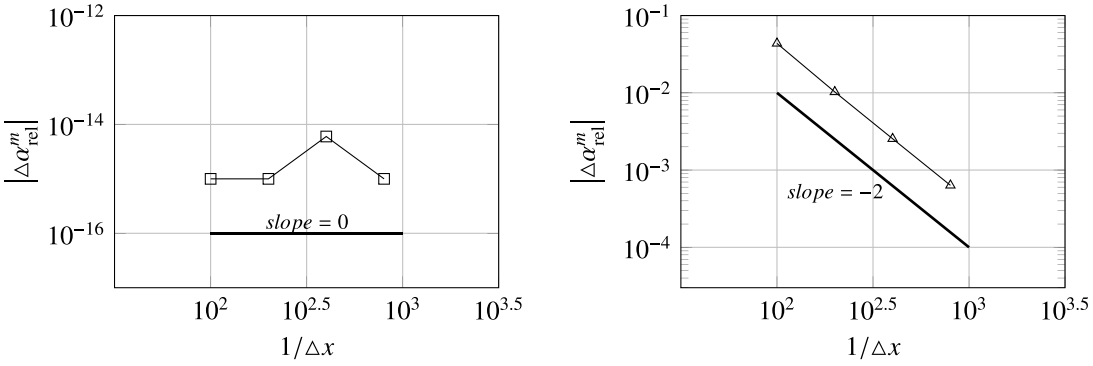

(a) Simulated concentration curve is used as the reference curve. (b) Analytical concentration curve is used as the reference curve.

Fig. 5. Comparison of the experimental order of convergence regarding the final relative error of the determined parameters for using simulative and analytical solution as the input.

First, the reference concentration curve is produced by a reference simulation using the reference parameters. The grid resolution of the LBM simulation is set equally in the reference simulation and during the optimization. This way, we can neglect several error sources such as discretization errors, boundary influences, or interpolation errors and can purely focus on the performance of the optimization framework. In Fig. 3, the evolution of the recovered isotherm constant is illustrated over the optimization steps. Therein, the reference value for the isotherm is depicted by the black solid line and it is shown that for all resolutions the parameter converges towards the reference parameter. Fig. 3 shows the relative error regarding the parameters and it is successfully demonstrated that the error decreases from initial $\approx 60\,\%$ to almost machine precision. Finally, Fig. 3 supports the findings by illustrating the decrease in the objective functional values over the conducted optimization steps. The perfect match of all curves in Fig. 3 demonstrates the grid independence of the optimization problem.

Next, the reference concentration curve is produced by the analytical solution given in (21). Thus, we now introduce discretization errors into the optimization problem. Fig. 4a shows that for increasing grid resolution the recovered isotherm parameter approaches the reference parameter. This is as expected as the discretization error is compensated by the reconstructed control parameter by the optimization framework. Analogously, we observe decreasing relative errors and objective values for increasing grid resolution in Fig. 4b and Fig. 4c.

In the previous work (Bukreev et al., 2023), the second order of convergence is demonstrated for this batch reactor case. Thus, the experimental order of convergence regarding the recovered parameters is computed, i.e., the relative error regarding the recovered parameters in the final optimization step is compared. Fig. 5a shows the results obtained where simulated reference curve is used. As shown above, there is no dependency between the grid resolution and the accuracy of the identified parameters observable in this case. However, Fig. 5b shows second order convergence of the relative error regarding the parameters meaning that in this case the same order of convergence is obtained as the simulated solute concentration curve compared to its analytical solution. As mentioned above, the results obtained by using simulated input data do not contain any influences of error sources besides the error introduced by the optimization algorithm. Thus, we use this input data for all further investigations to focus solely on the performance of the optimization framework.

3.3.2. *Identification of multiple parameters*

Next, the capability of determining more than a single parameter is investigated by adding the particle radius as an additional degree of freedom in our optimization problem. As the initial guess, the values from (25) are used. Fig. 6 shows the results for the simultaneous identification of the isotherm constant and the particle radius. Both, parameters are successfully recovered as shown for the actual control parameter values in Fig. 6a and by the decreasing relative error over the optimization steps in Fig. 6b. The development of the objective function supports the found results, given in Fig. 6c. Compared to the obtained results where only the isotherm constant is recovered, the number of required optimization steps to reach the same accuracy has been increased. However, the initial relative error of 67 % and 90 % for the isotherm and radius are reduced to almost machine precision.

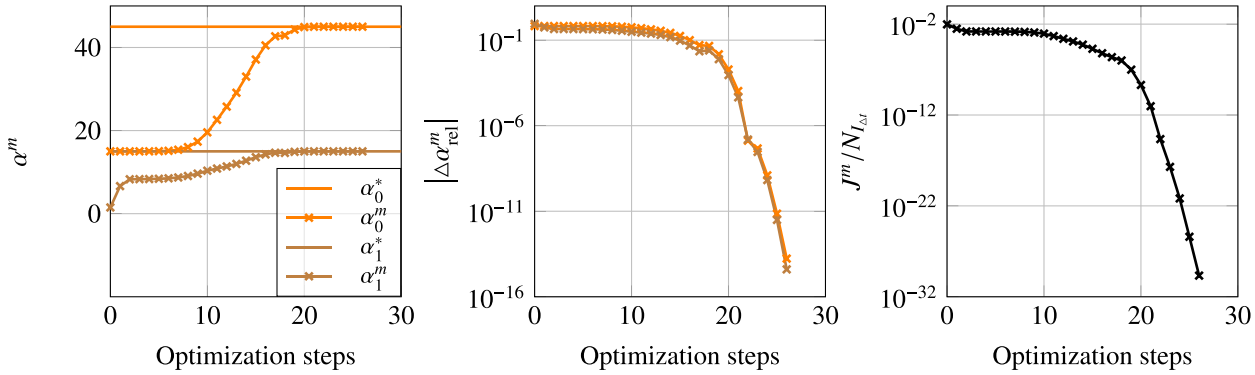

(a) Controls over optimization steps. (b) Rel. error controls over optimization steps. (c) Normed objective over optimization steps.

Fig. 6. Simultaneous identification of the isotherm constant and the particle radius.

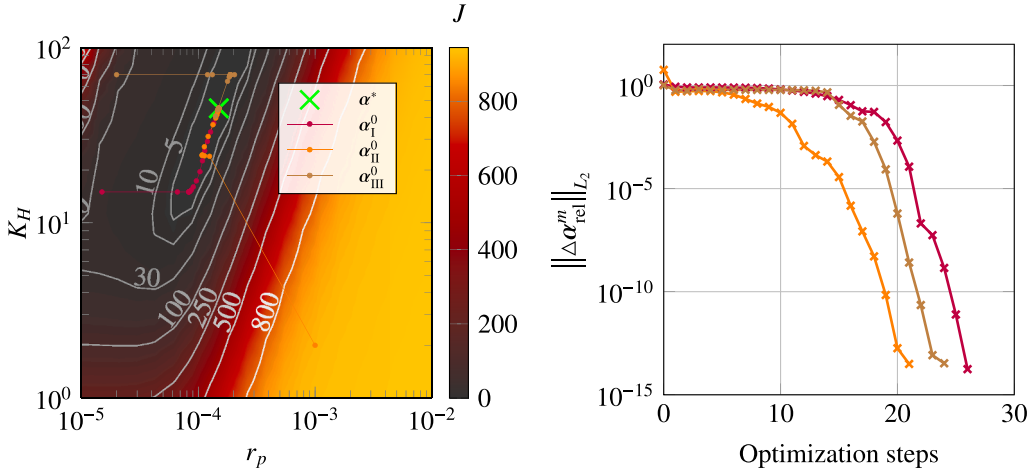

(a) Parameter evolution during optimization. (b) Rel. error controls over optimization steps.

Fig. 7. Investigation of various initial guesses for the optimization problem. 20×20 simulations are performed for $r_p \in [10^{-5}, 10^{-2}]$ and $K_H \in [1, 10^2]$ to produce the objective map on the left. Therein, the curves show the evolution of the recovered parameters over the optimization steps. The reference parameter set is highlighted by the green cross. On the right, the corresponding distance to the reference parameters from the current parameter over the optimization steps are plotted.

3.3.3. *Variation of the initial guess*

As a gradient-based approach is utilized in this work, the influence of the initial guess regarding the control parameters is a necessary aspect to be investigated. Therefore, three different initial guesses are tested if the reference parameters can be recovered which are given as

$$\boldsymbol{\alpha}_{\text{I}}^0 = \begin{pmatrix} 15 \\ 1.0 \times 10^{-5} \end{pmatrix}, \quad \boldsymbol{\alpha}_{\text{II}}^0 = \begin{pmatrix} 2 \\ 1.0 \times 10^{-3} \end{pmatrix}, \quad \boldsymbol{\alpha}_{\text{III}}^0 = \begin{pmatrix} 70 \\ 2.0 \times 10^{-5} \end{pmatrix}. \tag{28}$$

To gain further insights into the optimization problem, the objective function is evaluated on 20×20 points for various control parameter to illustrate the objective domain of the current adsorption problem. That is, 20 evenly distributed points on the logarithmic scale are computed for the isotherm constant and radius resulting in a total of 400 simulations. Therein, the developments of the recovered parameters for the different initial guess from (28) are depicted, all leading to the reference parameters, highlighted by the green mark in Fig. 7a. It can be seen, that for steep gradients large step sizes are computed showing the successful employment of the quasi-Newton method and the step size control. The results in Fig. 7b supports the findings by showing the distance to the reference parameters over the optimization steps and show that for various initial guesses the optimization framework can recover the reference parameters. In practical applications, the initial guess should be chosen by referring to existing literature to have a good estimate to start with.

3.3.4. *Influence of noise signals*

The long term goal is to apply this method on experimentally obtained concentration curves obtained by measurements. Therein, the presence of noise signals is unavoidable. Thus, the influence of different noise signal intensities on the input data is important to investigate. On the input concentration curve, artificially created Gaussian-distributed noise signals are added in each discrete time step. That is, the signal intensity is computed relative to the current solute concentration in each discrete time point. The noise intensity is given by the signal-to-noise ratio (SNR) given here as $\text{SNR} = 1/p$ where p is the percentage of the maximal possible noise signal amplitude. Fig. 8a depicts exemplary the noisy concentration curve with $\text{SNR} = 1$ together with the noise-free curve. Using this curve as the input, the isotherm constant is recovered by the optimization framework.

Fig. 8b shows the evolution of the relative error regarding the recovered parameters over the optimization steps. Therein, the final accuracy of the determined isotherm constant depends on the applied intensity of the noise signals. Even for a $\text{SNR} = 1$, the initial relative error of 67 % is reduced to 12 % which equals to a 5.6 times reduction of the initial error. For higher SNR such as $\text{SNR} = 5$, the final relative error contains only 2 % showing strong capabilities of the presented method. As a demonstration, the recovered solute concentration curve is illustrated in Fig. 8a for visual comparison with the noise-free and noisy concentration curve which has been used as the input data for the framework.

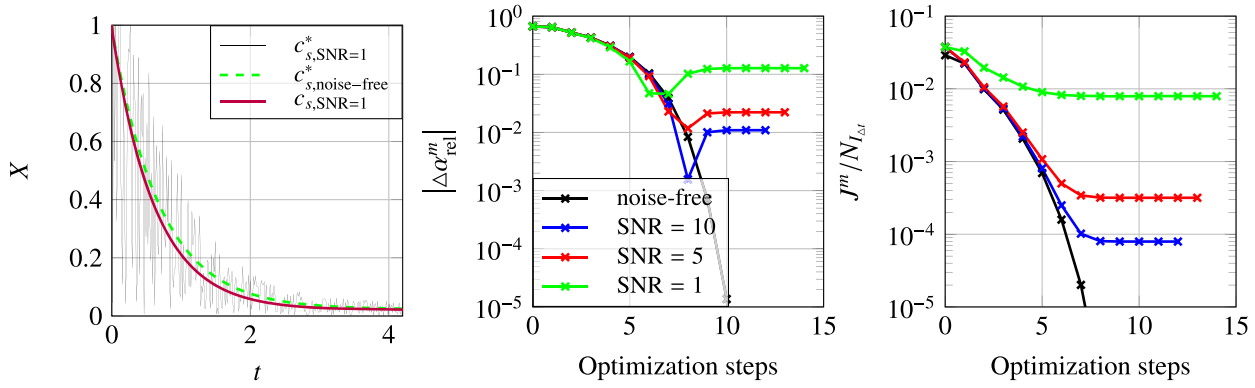

(a) Dimensionless solute concentration curves.

(b) Rel. error controls over optimization steps.

(c) Normed objective over optimization steps.

Fig. 8. ParamId simData twoParams.

4. Conclusion

In the presented manuscript, a numerical framework is proposed combining LBM simulations with gradient-based optimization algorithms to solve the parameter identification problem for adsorption models, e.g., adsorption isotherm constant and particle radius. This work is build on the previous results from Bukreev et al. (2023) and a benchmark case for the optimization problem is constructed for the batch reactor case. Therein, several aspects has been addressed such as the accuracy of the recovered parameters, robustness of the algorithm regarding different initial guesses and noise signals. The influence of the spatial resolution in the simulation for various input data sets is also analyzed where second order convergence is obtained for the identified parameters when using analytical solute concentration curve as the input. When simulated input data is used, the relative error is reduced to machine precision in 13 optimization steps for recovering one parameter and 26 optimization steps for two parameters simultaneously. The framework demonstrated reliability to determine the reference parameters when varying the initial guesses, where comprehensive investigations has been performed by mapping the objective functional for a wide range of control parameters. Finally, great results are achieved regarding the adaptivity of the algorithm on noise signals in the input data. That is, for a SNR $= 2$, the relative error regarding the isotherm constant is reduced from initial 67 % to 2 %. Similar results were obtained as in the work of Grigoriev et al. (2020) where conventional physical models have been applied, showing that the choice of the present models are capable of archiving accurate results in the parameter identification problem.

Supported by those results, we think the proposed framework is capable to determine model parameters when applied on real measurement data which will be the scope in future works. The constructed benchmark case is suited to address several aspects in the parameter identification problem with great flexibility for further more specific investigations. The framework is easily extendable for more complex adsorption processes as the whole algorithm is designed to work with different adsorption models or macroscopic target equations. All applied methods are implemented and all presented results are produced with the open source library OpenLB.

Data availability

Data will be made available on request.

Declaration of competing interest

The authors declare that they have no known competing financial interests or personal relationships that could have appeared to influence the work reported in this paper.

CRediT authorship contribution statement

Shota Ito: Writing – original draft, Validation, Methodology, Investigation, Formal analysis, Data curation, Conceptualization; **Simon Großmann:** Writing – review & editing, Validation, Methodology, Investigation, Formal analysis; **Fedor Bukreev:** Writing – review & editing, Formal analysis; **Julius Jeßberger:** Writing – review & editing, Software; **Mathias J. Krause:** Writing – review & editing, Resources, Funding acquisition

List of symbols

c_s	Simulated solute concentration
c^*_s	Reference solute concentration
$c_{s,0}$	Initial condition reg. solute concentrtaion
c_p	Simulated particle concentration
c_q	Simulated loading concentration
Ω	Spatial flow domain
$\Omega_{\triangle x}$	Spatially discretized flow domain
$\mathbf{x}$	Grid node position
$\mathbf{x}^*$	Reference data position
$\triangle x$	Grid step size
I	Time space
$I_{\triangle t}$	Discretized time space
t	Time
$\triangle t$	Time step
J	Optimization objective
$\mathbf{G}$	Optimization constraint
$\boldsymbol{\alpha}$	Vector of controls
$\boldsymbol{\alpha}^*$	Vector of reference parameters
α	Control parameter
α^*	Reference parameter
α^0	Initial guess reg. controls
$\left\|\triangle\alpha^m_{\mathrm{rel}}\right\|$	Rel. error reg. control
$\left\|\left\|\triangle\boldsymbol{\alpha}^m_{\mathrm{rel}}\right\|\right\|_{L_2}$	Rel. error reg. controls
$\mathbf{u}$	Fluid velocity
ρ	Fluid density
ν	Kinematic fluid viscosity
p	Pressure
S_{ads}	Source term modelling adsorption
D	Diffusivity constant
X	Dimensionless concentration
r_p	Particle radius
K_H	Henry-isotherm constant
q	Particle loading
q^{eq}	Equilibrium loading
D_s^{eq}	Surface diffusion constant

k_f	Film transport coefficient
k_s	Surface transport coefficient
T	Dimensionless time
f_i	Particle distribution function for NSE
g_i	Particle distribution function for ADE
f_i^{eq}	Quadratic equilibrium distribution
g_i^{eq}	Linear equilibrium distribution
w_i	Discretization weights
c_s	Speed of sound
τ	Relaxation time
D_b	Distribution factor

Acknowledgments

The current research is a part of the DFG project number 436212129 "Increase of efficiency in phosphate recovery by understanding the interaction of flow and loading processes with modeling and simulation". In addition, this project has received funding from the KIT Center for Mathematics in Sciences, Engineering and Economics under the seed funding program.

The authors thank Stephan Simonis for valuable comments.

Appendix A. Simulation and material parameters

Table A.1
Process parameters for the batch reactor case.

Parameter		Value	Unit
Isotherm parameter	K_H	45	L/g
Initial concentration	c_0	1	mg/L
Particle concentration	c_p	0.94	kg/m^3
Column length	L	0.1	m
Particle radius	r_p	$1.5 \cdot 10^{-4}$	m
Surface diffusion coefficient	D_s^{eq}	$5 \cdot 10^{-11}$	m^2/s^2

References

Berg, U., Knoll, G., Kaschka, E., Kreutzer, V., Donnert, D., Weidler, P.G., Nüesch, R., 2005. P-roc-phosphorus recovery from wastewater by crystallisation of calcium phosphate compounds. J. Residuals Sci. Technol. 4 (3).

Bhatnagar, P.L., Gross, E.P., Krook, M., 1954. A model for collision processes in gases. i. small amplitude processes in charged and neutral one-component systems. Phys. Rev. 94 (3), 511–525. https://doi.org/10.1103/PhysRev.94.511

Bonvin, D., 1998. Optimal operation of batch reactors—a personal view. J. Process Control 8 (5–6), 355–368. https://doi.org/10.1016/S0959-1524(98)00010-9

Bukreev, F., Raichle, F., Nirschl, H., Krause, M.J., 2023. Simulation of adsorption processes on moving particles based on an Euler-Euler description using a lattice Boltzmann discretization. Chem. Eng. Sci. 270, 118485. https://doi.org/10.1016/j.ces.2023.118485

Byrd, R.H., Lu, P., Nocedal, J., Zhu, C., 1995. A limited memory algorithm for bound constrained optimization. SIAM J. Sci. Comput. 16 (5), 1190–1208. https://doi.org/10.1137/0916069

Dapelo, D., Simonis, S., Krause, M.J., Bridgeman, J., 2021. Lattice-Boltzmann coupled models for advection–diffusion flow on a wide range of péclet numbers. J. Comput. Sci. 51, 101363. https://doi.org/10.1016/j.jocs.2021.101363

Glueckauf, E., Coates, J.I., 1947. Theory of chromatography; the influence of incomplete equilibrium on the front boundary of chromatograms and on the effectiveness of separation. J. Chem. Soc. (0), 1315–1321. https://doi.org/10.1039/JR9470001315

Griewank, A., Walther, A., 2009. Evaluating Derivatives: Principles and Techniques of Algorithmic Differentiation. Soc. for Industrial and Applied Mathematics, Philadelphia. 2nd rev. ed. edition.

Grigoriev, V.V., Iliev, O., Vabishchevich, P.N., 2020. Computational identification of adsorption and desorption parameters for pore scale transport in periodic porous media. J. Comput. Appl. Math. 370, 112661. https://doi.org/10.1016/j.cam.2019.112661

Gruszczyński, G., Dzikowski, M., Łaniewski-Wołłk, Ł., 2023. Revisiting the second-order convergence of the lattice Boltzmann method with reaction-type source terms. Comput. Math. Appl. 144, 34–50. https://doi.org/10.1016/j.camwa.2023.\protect\penalty-\@M05.020

Guo, Z., Shi, B., Zheng, C., 2002. A coupled lattice BGK model for the boussinesq equations. Int. J. Numer. Methods Fluids 39 (4), 325–342. https://doi.org/10.1002/fld.337

Hashimoto, K., Miura, K., 1976. A simplified method to design fixed-bed adsorbers for the freundlich isotherm. J. Chem. Eng. Jpn. 9 (5), 388–392. https://doi.org/10.1252/jcej.9.388

Ito, S., Jeßberger, J., Simonis, S., Bukreev, F., Kummerländer, A., Zimmermann, A., Thäter, G., Pesch, G.R., Thöming, J., Krause, M.J., 2024. Identification of reaction rate parameters from uncertain spatially distributed concentration data using gradient-based PDE constrained optimization. Comput. Math. Appl. 167, 249–263. https://doi.org/10.1016/j.camwa.2024.05.026

Jeßberger, J., Marquardt, J.E., Heim, L., Mangold, J., Bukreev, F., Krause, M.J., 2022. Optimization of a micromixer with automatic differentiation. Fluids 7 (5), 144. https://doi.org/10.3390/fluids7050144

Joshi, N., Ojha, C.S.P., Sharma, P.K., Surampalli, R.Y., 2013. Parameter identification of virus transport in porous media using equilibrium and non-equilibrium models. J. Environ. Chem. Eng. 1 (4), 1099–1107. https://doi.org/10.1016/j.jece.2013.08.023

Klemens, F., Förster, B., Dorn, M., Thäter, G., Krause, M.J., 2020a. Solving fluid flow domain identification problems with adjoint lattice Boltzmann methods. Comput. Math. Appl. 79 (1), 17–33. https://doi.org/10.1016/j.camwa.2018.07.010

Klemens, F., Schuhmann, S., Balbierer, R., Guthausen, G., Nirschl, H., Thäter, G., Krause, M.J., 2020b. Noise reduction of flow MRI measurements using a lattice Boltzmann based topology optimisation approach. Comput. Fluids 197, 104391. https://doi.org/10.1016/j.compfluid.2019.104391

Klemens, F., Schuhmann, S., Guthausen, G., Thäter, G., Krause, M.J., 2018. Cfd-mri: a coupled measurement and simulation approach for accurate fluid flow characterisation and domain identification. Comput. Fluids 166, 218–224. https://doi.org/10.1016/j.compfluid.2018.02.022

Krause, M.J., Heuveline, V., 2013. Parallel fluid flow control and optimisation with lattice Boltzmann methods and automatic differentiation. Comput. Fluids 80, 28–36. https://doi.org/10.1016/j.compfluid.2012.07.026

Krause, M.J., Kummerländer, A., Avis, S.J., Kusumaatmaja, H., Dapelo, D., Klemens, F., Gaedtke, M., Hafen, N., Mink, A., Trunk, R., Marquardt, J.E., Maier, M.-L., Haussmann, M., Simonis, S., 2021. OpenLB—open source lattice oltzmann code. Comput. Math. Appl. 81, 258–288. https://doi.org/10.1016/j.camwa.2020.04.033

Krause, M.J., Thäter, G., Heuveline, V., 2013. Adjoint-based fluid flow control and optimisation with lattice Boltzmann methods. Comput. Math. Appl. 65 (6), 945–960. https://doi.org/10.1016/j.camwa.2012.08.007

Kummerländer, A., Bingert, T., Bukreev, F., Czelusniak, L.E., Dapelo, D., Hafen, N., Heinzelmann, M., Ito, S., Jeßberger, J., Kusumaatmaja, H., Marquardt, J.E., Rennick, M., Pertzel, T., Prinz, F., Sadric, M., Schecher, M., Simonis, S., Sitter, P., Teutscher, D., Zhong, M., Krause, M.J., 2024. OpenLB release 1.7: Open source lattice Boltzmann code. https://doi.org/10.5281/ZENODO.10684609

Liu, D.C., Nocedal, J., 1989. On the limited memory BFGS method for large scale optimization. Math. Program. 45 (1–3), 503–528. https://doi.org/10.1007/BF01589116

Seta, T., 2013. Implicit temperature-correction-based immersed-boundary thermal lattice Boltzmann method for the simulation of natural convection. Phys. Rev. E Stat. Nonlin. Soft Matter Phys. 87 (6), 063304. https://doi.org/10.1103/PhysRevE.87.063304

Simonis, S., 2023. Lattice Boltzmann methods for partial differential equations. https://doi.org/10.5445/IR/1000161726

Simonis, S., Frank, M., Krause, M.J., 2020. On relaxation systems and their relation to discrete velocity Boltzmann models for scalar advection-diffusion equations. Philos. Trans. A Math. Phys. Eng. Sci. 378 (2175), 20190400. https://doi.org/10.1098/rsta.2019.0400

Simonis, S., Frank, M., Krause, M.J., 2023. Constructing relaxation systems for lattice Boltzmann methods. Appl. Math. Lett. 137, 108484. https://doi.org/10.1016/j.aml.2022.108484

Simonis, S., Haussmann, M., Kronberg, L., Dörfler, W., Krause, M.J., 2021. Linear and brute force stability of orthogonal moment multiple-relaxation-time lattice Boltzmann methods applied to homogeneous isotropic turbulence. Philos. Trans. A Math. Phys. Eng. Sci. 379 (2208), 20200405. https://doi.org/10.1098/rsta.2020.0405

Simonis, S., Krause, M.J., 2022. Limit consistency of lattice Boltzmann equations. http://arxiv.org/pdf/2208.06867.

Wang, L., Shi, B., Chai, Z., 2015. Regularized lattice Boltzmann model for a class of convection-diffusion equations. Phys. Rev. E 92, 043311. https://doi.org/10.1103/PhysRevE.92.043311

Worch, E., 2008. Fixed-bed adsorption in drinking water treatment: a critical review on models and parameter estimation. J. Water Supply Res. Technology-Aqua 57 (3), 171–183. https://doi.org/10.2166/aqua.2008.100

Worch, E., 2012. Adsorption Technology in Water Treatment. De Gruyter. https://doi.org/10.1515/9783110240238

Worch, E., 2021. Adsorption Technology in Water Treatment. De Gruyter. https://doi.org/10.1515/9783110715507

Yoshida, H., Nagaoka, M., 2010. Multiple-relaxation-time lattice Boltzmann model for the convection and anisotropic diffusion equation. J. Comput. Phys. 229 (20), 7774–7795. https://doi.org/10.1016/j.jcp.2010.06.037